

Polymer Translocation Dynamics in the Quasi-Static Limit

James M. Polson and Anthony C. M. McCaffrey¹

Department of Physics, University of Prince Edward Island, 550 University Ave., Charlottetown, Prince Edward Island, C1A 4P3, Canada

(Dated: 21 March 2013)

Monte Carlo (MC) simulations are used to study the dynamics of polymer translocation through a nanopore in the limit where the translocation rate is sufficiently slow that the polymer maintains a state of conformational quasi-equilibrium. The system is modeled as a flexible hard-sphere chain that translocates through a cylindrical hole in a hard flat wall. In some calculations, the nanopore is connected at one end to a spherical cavity. Translocation times are measured directly using MC dynamics simulations. For sufficiently narrow pores, translocation is sufficiently slow that the mean translocation time scales with polymer length N according to $\langle\tau\rangle \propto (N - N_p)^2$, where N_p is the average number of monomers in the nanopore; this scaling is an indication of a quasi-static regime in which polymer-nanopore friction dominates. We use a multiple-histogram method to calculate the variation of the free energy with Q , a coordinate used to quantify the degree of translocation. The free energy functions are used with the Fokker-Planck formalism to calculate translocation time distributions in the quasi-static regime. These calculations also require a friction coefficient, characterized by a quantity N_{eff} , the effective number of monomers whose dynamics are affected by the confinement of the nanopore. This was determined by fixing the mean of the theoretical distribution to that of the distribution obtained from MC dynamics simulations. The theoretical distributions are in excellent quantitative agreement with the distributions obtained directly by the MC dynamics simulations for physically meaningful values of N_{eff} . The free energy functions for narrow-pore systems exhibit oscillations with an amplitude that is sensitive to the nanopore length. Generally, larger oscillation amplitudes correspond to longer translocation times.

I. INTRODUCTION

The translocation of a polymer through a narrow passage from one space to another is a fundamental process with numerous applications.¹ It is a key part of various biological phenomena, including viral genome transfer, RNA transport through the nuclear pore complex, protein transport into mitochondria, and genome packing in bacteriophages.^{2,3} The pioneering work of Kasianowicz *et al.* first demonstrated the feasibility of monitoring translocation of single molecules by measurement of the ionic current passing through nanometre-sized pores.^{4,5} In this method, the potential difference that drives the ionic current also drives a charged macromolecule through a nanopore, and the translocation results in a measurable reduction in the current. Substantial effort has been devoted to further develop this experimental technique using both biological^{6–12} and synthetic nanopores.^{13–19} This work has largely been motivated by the desire to develop a fast and inexpensive method of sequencing DNA.^{20–22} The experiments have revealed a complex dependence of translocation behaviour on a variety of factors, including electric field strength,¹⁷ pH,¹² and salt concentration.²³ An understanding of this growing body of experimental results is currently incomplete.¹

Numerous theoretical and computer simulation studies of polymer translocation have been reported in recent years. Much of this work has been summarized and evaluated in a recent review.²⁴ One notable theoretical approach, pioneered by Sung and Park²⁵ and Muthukumar²⁶ employs the Fokker-Planck (FP) formalism. Here, the dynamics are governed by the free en-

ergy, $F(s)$, which is a function of a single coordinate, s , typically defined to be the number of monomers on one side the nanopore. The time-dependent probability distribution for this coordinate is obtained by solving a 1-D Smoluchowski equation, for which the free energy function is required input. This solution can be used to calculate translocation time distributions and determine scaling relations for mean translocation times. The predicted scaling relations are quantitatively consistent with results from experiments of DNA translocation through α -hemolysin.^{1,26} The FP formalism has been used to study translocation to various levels of approximation and for different confinement geometries.^{11,27–36} A detailed review of the FP formalism and its application to polymer translocation is provided in the recent book by Muthukumar.¹

The veracity of the free energy functions clearly determines the accuracy of the predictions for translocation dynamics in the FP approach. Most FP theoretical studies employ analytical approximations of $F(s)$ ^{11,25,26,28–33,37–39} In other studies, the free energies have been calculated numerically for specific molecular models that can also be employed in dynamics simulations. For example, exact enumeration of polymer configurations has been used to calculate a free energy landscape in order to elucidate the effects of polymer-nanopore attractions on translocation times for a lattice model system.^{41,42} Off-lattice models have been studied using specialized Monte Carlo simulation methods. One recent example is the incremental gauge cell (IGC) method,⁴³ which was used to calculate free energy profiles for a flexible Lennard-Jones chain translocating out of a spherically confined space with adsorbing walls.³⁴

Another efficient MC method appropriate to calculate translocation free energies is the self-consistent multiple histogram (SCMH) technique.⁴⁴ Recently, we used the SCMH method to calculate free energy functions for flexible hard-sphere chains translocating through a cylindrical pore in a hard barrier.^{45,46} Generally, the free energy curves follow trends that conform well to the predictions of a modified version of the standard analytical model described in Ref. 1. However, one unexpected feature observed was an oscillation in the free energy with an amplitude that is very sensitive to the nanopore dimensions.⁴⁶ While its relevance to the experimental context is unclear, knowledge of such effects may be helpful for the interpretation of results from dynamics simulations and could be relevant to elucidating the sensitivity of the translocation behaviour on seemingly minor differences in the model that have been observed in some simulation studies.^{77,85,86}

The validity of the FP approach to polymer translocation is founded on the assumption that the portions of the polymer outside the pore remain in conformational equilibrium during the entire translocation process. This is expected to be the case in the limit of sufficiently strong pore friction for polymers of finite length. In this case the translocation time scales as N^2 for unbiased translocation^{26,39} and as N/f for forced translocation,²⁶ where f is the driving force magnitude. However, it is well known that this assumption must break down for sufficiently long polymers.^{47,48} Computer simulation studies have generally yielded scaling exponents inconsistent with the values for the quasi-static regime with strong pore friction.^{47–53,59,62–78} The values of the exponents vary widely and appear to be sensitive to the details of the model, simulation method, and the length of the polymer. In addition, nonequilibrium conformational behaviour has been observed directly.^{58,74,75,79–82} Various theoretical models have been developed to account for non-equilibrium effects and generally predict scaling exponent values greater than those for the quasi-equilibrium case, both for nondriven^{49–51} and driven^{52–61} translocation. Clearly, the FP formalism is an inappropriate approach for the conditions considered in most of these simulation studies. However, simulation models can easily be adjusted to either reduce the relaxation time of the chain or increase the nanopore friction, either of which should eventually lead to quasi-static conditions. This is illustrated by a recent simulation study of unforced translocation that followed the former approach and measured a scaling exponent value consistent with FP predictions for the quasi-static regime at sufficiently low viscosity where the relaxation time of the chain is very short.⁵¹

The purpose of this study is to examine the accuracy with which the FP formalism describes the translocation dynamics in the quasi-static regime. The system is modelled as freely-jointed hard-sphere chain that translocates through a cylindrical nanopore in a hard barrier. We employ free energy functions that were calculated using

the SCMH method in our recent study.⁴⁶ The calculated translocation time distributions are compared to those measured directly from MC dynamics calculations for the same model. Calculations were carried out for systems in the quasi-static regime with friction dominated by the nanopore. The regime boundary is determined by measurement of the scaling exponent in MC dynamics simulations. The friction coefficient used in the FP calculations is characterized by a parameter N_{eff} , the effective number of monomers whose dynamics are affected by nanopore confinement. We focus mainly on a system with a planar barrier and semi-infinite *cis* and *trans* spaces. We also present some results for the cases where the pore is connected to a spherical cavity at one end; comparable systems have been the focus of a number of other theoretical and computer simulation studies.^{27,28,30,32,33,83,84} We investigate the effects on the translocation dynamics of varying the nanopore dimensions, the initial position of the polymer, and polymer length. Generally, the theoretical distributions are in excellent quantitative agreement with those measured from MC dynamics simulations for physically meaningful values of N_{eff} .

The remainder of this article is organized as follows. In Section II, the model is described. In Section III, we present a brief overview of the relevant results of the FP methodology and describe how the friction coefficient employed in the theory is calculated. In Section IV, we describe the MC algorithm used in the dynamics simulations and the details of the FP calculations. In Section V, the simulation results are presented, and the significance of the results is discussed in Section VI.

II. MODEL

The polymer is modeled as a flexible chain of N hard spheres, each with a diameter of σ . The pair potential for nonbonded monomers is thus

$$u_{\text{nb}}(r) = \begin{cases} \infty, & r < \sigma \\ 0, & r > \sigma, \end{cases} \quad (1)$$

where r is the distance between the centres of the monomers. Pairs of bonded monomers interact with a potential

$$u_{\text{b}}(r) = \begin{cases} 0, & 0.9\sigma < r < 1.1\sigma \\ \infty, & \text{otherwise.} \end{cases} \quad (2)$$

Thus, the bond length can fluctuate slightly about its average value, which is equal to the monomer diameter.

The polymer undergoes translocation through a narrow pore from one region to another. The nanopore is modeled as a cylindrical hole of length L and radius R in a hard barrier. The regions on the two sides of the nanopore are labeled *cis* and *trans*. Two different cases are considered in this study. In the first case, the *cis* and *trans* sides are semi-infinite spaces, and the barrier that separates them is bounded by two flat surfaces.

Monomers cannot overlap with the barrier, and thus the minimum distance between the centre of a monomer and the nearest point on either the barrier wall surface or the nanopore surface is $\sigma/2$. This confinement geometry is illustrated in Fig. 1(a). In the second case, translocation occurs between a spherical cavity of radius R_c on the *cis* side to a semi-infinite space on the *trans* side, as shown in Fig. 1(b). Most of the calculations in this study employed the first variant of the model.

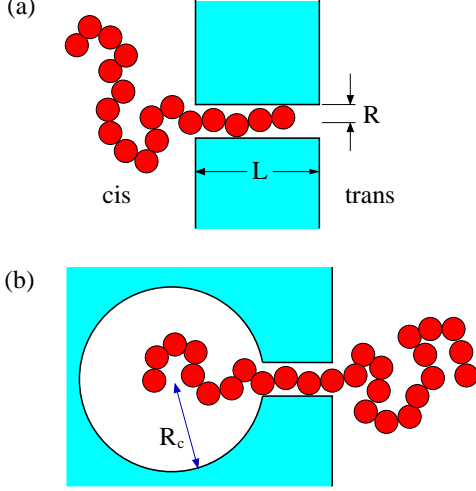


FIG. 1. Illustration of the two confinement geometries employed in this study. Most of the calculations in this study used the system shown in (a).

The degree to which the polymer has translocated across the nanopore is quantified using a translocation coordinate, Q , which is defined:

$$Q = \frac{1}{N} \sum_{i=1}^N Q_i, \quad (3)$$

where the translocation coordinate for the i th monomer is given by

$$Q_i = \begin{cases} 0, & z_i < 0 \\ z_i/L, & 0 < z_i < L \\ 1, & z_i > L \end{cases} \quad (4)$$

where z_i is the z -coordinate for the i th monomer. Thus, $Q = 0$ when all monomers are on the *cis* side of the pore, $Q = 1$ when the polymer is completely on the *trans* side, and $0 < Q < 1$ if there are any monomers inside the nanopore. Clearly, Q is a continuous quantity, which makes it a more convenient choice for a translocation coordinate here than the quantity s (the number of monomers on the *trans* side of the pore) used in most translocation studies.

III. THEORETICAL BACKGROUND

In the quasi-static limit, the time-dependent translocation probability distribution, $\mathcal{P}(Q, t)$, is governed by the Fokker-Planck equation. When the pore friction is dominant contribution to the total polymer friction the form of the equation is¹

$$\frac{\partial \mathcal{P}}{\partial t} = D \left[\frac{\partial}{\partial Q} \left(\frac{1}{k_B T} \frac{\partial F}{\partial Q} \mathcal{P}(Q, t) \right) + \frac{\partial^2 \mathcal{P}(Q, t)}{\partial Q^2} \right], \quad (5)$$

where k_B is Boltzmann's constant, T is temperature, $F(Q)$ is the equilibrium translocation free energy function and D is an effective diffusion coefficient. Consider a domain bounded by $Q = Q_a$ and $Q = Q_b$. The first passage time, τ , for a polymer located at $Q_0 \in [Q_a, Q_b]$ at time $t = 0$ to reach either boundary has a probability distribution given by¹

$$g(\tau; Q_0) = -\frac{d}{d\tau} \int_{Q_a}^{Q_b} dQ p(Q, \tau; Q_0, 0), \quad (6)$$

where $p(Q, t; Q', t')$ is the conditional probability of the polymer reaching a value Q at time t given that it had a value of Q' at an earlier time t' . For a Markov process, $p(Q, t; Q', t')$ also satisfies Eq. (5). In the case of absorbing boundary conditions the mean first passage time is given by:¹

$$\langle \tau \rangle = \frac{\left(\int_{Q_0}^{Q_b} \frac{dy}{\psi(y)} \right) \int_{Q_a}^{Q_0} \frac{dy'}{\psi(y')} H(y') - \left(\int_{Q_a}^{Q_0} \frac{dy}{\psi(y)} \right) \int_{Q_0}^{Q_b} \frac{dy'}{\psi(y')} H(y')}{\int_{Q_a}^{Q_b} \frac{dy}{\psi(y)}}, \quad (7)$$

where

$$\psi(Q) = \exp(-[F(Q) - F(Q_a)]/k_B T). \quad (8)$$

and

$$H(Q) = -D^{-1} \int_{Q_a}^Q dQ' \psi(Q') \quad (9)$$

Finally, the probability a polymer reaches $Q = Q_b$ without ever reaching Q_a is given by:¹

$$\pi_b(Q_0) = \frac{\Psi(Q_a, Q_0)}{\Psi(Q_a, Q_b)} \quad (10)$$

where

$$\Psi(x, y) \equiv \int_x^y \frac{dz}{\psi(z)} \quad (11)$$

Note that this probability depends only on the free energy function and not on the diffusion coefficient.

In order to calculate $g(\tau; Q_0)$ and $\langle \tau \rangle$, the free energy function, $F(Q)$, and the diffusion coefficient D must be supplied. In this study, $F(Q)$ is calculated using the SCMh method, as described in Ref. 46. The diffusion coefficient D is closely related to the diffusion coefficient of monomers confined by the nanopore. In this study, we employ a MC method to study the translocation dynamics of the polymer; the details of the method will be described below in Section IV B. The diffusion rate for monomers inside the nanopore is determined by nature of the MC trial moves for the individual monomers. Unfortunately, quantitatively accurate values of D cannot easily be calculated analytically from knowledge of the details of the model and method alone. Consequently, the diffusion coefficient is essentially treated as a free parameter. However, it is possible to determine the scaling of D with polymer length and (approximately) with nanopore length in the limit of strong pore friction.

Consider a polymer that moves inside an infinitely long cylindrical tube aligned along the z axis. The polymer diffuses along z such that its mean square displacement satisfies

$$\langle \Delta z^2 \rangle = 2D_z t = \frac{2k_B T}{\gamma_z} t \quad (12)$$

where $D_z = k_B T / \gamma_z$ is the diffusion coefficient and γ_z is the friction coefficient associated with the polymer inside the tube. In this study, we consider the model polymer described in Section II that moves via random displacements of randomly chosen monomers, one at a time. In this case, the friction coefficient in Eq. (12) scales as

$$\gamma_z = \gamma_0(N - 1), \quad (13)$$

where N is the number of monomers. In addition, γ_0 is a constant that depends on the radius of the tube and the probability distribution of trial monomer displacements employed in the calculations. This scaling relation is confirmed through results from simulations. Now consider a polymer undergoing translocation through a cylindrical nanopore of finite length, L . For a sufficiently narrow pore, the pore friction is expected to be the dominant contribution to the overall friction of the polymer. In this case, the friction coefficient governing the motion along z for the portion of the polymer inside the pore is expected to obey a relation similar Eq. (13),

$$\gamma_z = \gamma_0(N_{\text{eff}} - 1), \quad (14)$$

where N_{eff} is the effective number of monomers whose dynamics are strongly effected by the presence of the nanopore. To estimate N_{eff} , first note that the range over which monomers are subject to some degree of confinement is $L + \sigma$. For a narrow nanopore, the polymer is approximately linear inside the pore and the

number of bonds spanning the confinement region is $n_{\text{bond}} = (L + \sigma)/\sigma$; thus, the number of monomers spanning this region can be estimated as $N_{\text{eff}} \approx n_{\text{bond}} + 1$, or

$$N_{\text{eff}} \approx L/\sigma + 2. \quad (15)$$

In practice, N_{eff} is a free parameter, albeit one that should come close to satisfying the approximation in Eq. (15).

In the absence of a free energy gradient, and for sufficiently strong pore friction, the mean square displacement for monomers inside the nanopore is expected to obey Eq. (12). From the definition of Q in Eqs. (3) and (4) it follows that a pore monomer displacement of Δz corresponds to a translocation coordinate change of $\Delta Q = \Delta z / (N\sigma)$, on average. Consequently, $\langle \Delta Q^2 \rangle = 2Dt$, where

$$D = \frac{k_B T}{\gamma}, \quad (16)$$

and where $\gamma = N^2 \gamma_z$. D is the diffusion coefficient that appears in Eq. (5), and γ is the corresponding friction coefficient. It follows that

$$\gamma = N^2 \gamma_0 (N_{\text{eff}} - 1). \quad (17)$$

The quantity N_{eff} is mainly determined by the nanopore length and can be approximated using Eq. (15). The quantity γ_0 is governed by the specifics of the MC dynamics algorithm. In practice, it can be determined from MC measurements of the time-dependence of $\langle \Delta z^2 \rangle$ for polymers of different lengths confined to an infinite cylindrical tube.

IV. METHODS

A. Free Energy Calculations

Monte Carlo simulations employing the Metropolis algorithm and the self-consistent multiple histogram (SCMH) method⁴⁴ were used to calculate the free energy functions for the polymer-nanopore model described in Section II. The results of these calculations were presented in a recent article,⁴⁶ to which the reader should refer for a detailed description of the methodology.

B. MC Dynamics Simulations

Monte Carlo dynamics simulations were used to study the translocation dynamics for the system. Polymer motion was generated through random monomer displacement, in which the coordinates of a randomly chosen monomer were displaced by an amount Δr_λ for $\lambda = x, y, z$. Each coordinate displacement was randomly chosen from a uniform distribution $[-\Delta_{\text{max}}, \Delta_{\text{max}}]$. Unless otherwise stated, $\Delta_{\text{max}} = 0.14\sigma$. A trial moves was

rejected if it lead to overlap with another nonbonded monomer, violation of the bonding constraint, or overlap with the nanopore or barrier wall. The polymer coordinates were chosen to correspond a desired initial coordinate, Q_0 , and the system was equilibrated for fixed Q_0 for typically 10^6 MC cycles. Two different first passage times were measured: (1) τ_1 , the first time that all monomers had completely emptied from either the *cis* or *trans* domain, and (2) τ , the first time that all monomers had completely emptied the nanopore and were all in either the *cis* or *trans* region. We define τ_2 to be the time taken by the polymer to empty the nanopore, and thus, $\tau = \tau_1 + \tau_2$. We simulated typically 500 – 2000 translocation events to calculate mean translocation times and $10^4 - 10^5$ events in cases where translocation time distributions were desired.

C. Theoretical Calculations

MC dynamics simulations of a hard-sphere chain polymer in an infinitely long cylinder were used to measure $\langle \Delta z^2 \rangle$ as a function of time for the centre of mass of a polymer for several lengths. A linear fit to each of these functions was used to extract the friction coefficient γ_z using Eq. (12). Fitting γ_z vs polymer length using Eq. (13) yielded the constant γ_0 for a tube of a specified radius.

Equations (7), (8) and (9) were used to calculate the mean first passage time for the translocation events. The integrals were calculated numerically using the trapezoid rule. The friction coefficient γ was calculated using Eq. (17), and the corresponding diffusion coefficient, D , was then calculated using Eq. (16). The value of the effective number of monomers in the nanopore, N_{eff} , was chosen so that the calculated $\langle \tau_1 \rangle$ was equal to the value measured directly in the MC dynamics simulations. After determining D , Eq. (5) was solved numerically using a simple finite-difference method with the boundary condition $Q = Q_0$ at $t = 0$ to yield the function $\mathcal{P}(Q, t)$. The distribution of first passage times, $g(\tau; Q_0)$ was calculated by solving Eq. (6); the integral was first solved numerically using the trapezoid rule, and the derivative was calculated using the finite-difference approximation.

In the results presented below, lengths are measured in units of σ , the monomer diameter. In addition, time is measured in MC cycles, where 1 MC cycle corresponds to one attempted move per monomer, on average.

V. RESULTS

The focus of this study is the elucidation of polymer translocation dynamics in the quasi-static regime. In this regime, the FP formalism described in the previous section is valid and can be used to calculate first passage times associated with translocation. For a given model system, it is not clear *a priori* which parameter values

correspond to this regime. One effective means to delineate the regime boundaries is to measure the scaling exponent α , defined by the power law scaling relation:

$$\langle \tau \rangle \propto N^\alpha. \quad (18)$$

In the limit of sufficiently strong pore friction, where the system is in the quasi-static regime, it is expected that $\alpha = 2$ for unforced translocation. For a nanopore of finite length L , the most appropriate scaling relation is slightly different. For a narrow nanopore where the polymer has a linear configuration inside the nanopore, the appropriate relation is:

$$\langle \tau \rangle \propto (N - N_p)^\alpha, \quad (19)$$

where

$$N_p \equiv L/\sigma + 1 \quad (20)$$

is approximately the number of monomers that lie inside the nanopore. The rationale for this modification is that most of the time for translocation passes during the phase in which the nanopore is filled, and monomers lie outside in both the *cis* and *trans* regions, while the time elapsed during the pore-emptying stage is very small, by comparison. Thus, translocation is almost complete by the time either the *cis* or *trans* region first empties at time τ_1 , and $\tau = \tau_1 + \tau_2 \approx \tau_1$, since $\tau_2 \ll \tau_1$. Justification for this claim will be presented below. From this perspective, the effective length of the polymer is $N - N_p$. Of course, in the limit that $N \gg N_p$, Eq. (19) reduces to Eq. (18).

It is instructive to first compare the scaling results in this MC dynamics study with those from the Langevin dynamics study of Ref. 77, which examined polymer translocation through a hole in a flat two dimensional barrier. Because of the variability of bond lengths permitted by Eq. (2), we choose a small, but finite, barrier width of $L = 0.1$. This precludes the unphysical possibility that two bonded monomers are bisected by the wall away from the pore. This barrier width should be small enough to approximate a 2-D barrier. Figure 2 shows the mean translocation time $\langle \tau \rangle$ vs polymer length N for several different pore radii. In these simulations, the polymer was initially placed midway in the nanopore such that $Q_0 = 0.5$. Over the range of N considered ($N = 20-100$) $\langle \tau \rangle$ satisfies the power relation of Eq. (18). The solid curves show the best fits to the simulation data. The inset of the figure shows the corresponding values of the scaling exponents, α , as a function of pore radius, R . The exponent has a value of $\alpha \approx 2.4$ in the range $R = 0.65-0.9$, but decreases rapidly with decreasing R for $R < 0.65$ and reaches $\alpha = 2.07 \pm 0.01$ for $R = 0.525$. These data are in general agreement with the results of Ref. 77. Note that this scaling behaviour cannot be extrapolated to very large N . As N increases, the scaling is expected to change in a manner such that $\langle \tau \rangle$ increases monotonically with decreasing R .

Figure 3 shows similar scaling data for a nanopore of length $L = 2.917$. As in the case described above, decreasing R results in an increase in $\langle \tau \rangle$. Consequently, the

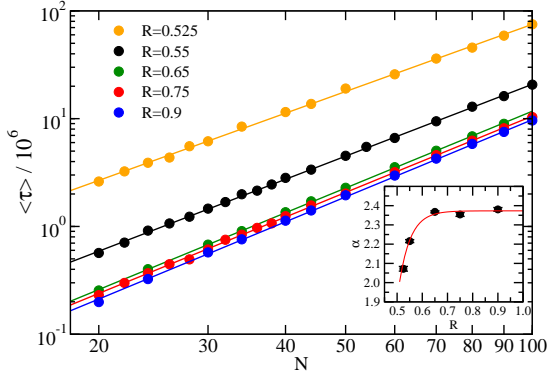


FIG. 2. Mean translocation time, $\langle \tau \rangle$, vs polymer length, N , for a pore of length $L = 0.1$ for several different pore radii. The inset shows the scaling exponent, α , vs pore radius R obtained from fits to the data. The solid red curve is a guide for the eye.

polymer can more easily maintain a state of conformational equilibrium as translocation proceeds, which leads to the observed decrease in the scaling exponent with R . The scaling exponent reaches a value of $\alpha = 2.003 \pm 0.004$ for a nanopore radius of $R = 0.55$, which corresponds to the case of quasi-static dynamics and strong pore friction.

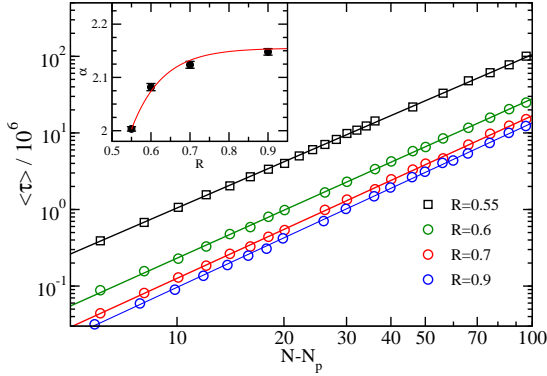


FIG. 3. Mean translocation time, $\langle \tau \rangle$, vs $N - N_p$, for a pore of length $L = 2.917$ for several different pore radii. The inset shows the scaling exponent, α , vs pore radius R obtained from fits to the data. The solid red curve is a guide for the eye.

One reason that decreasing the pore radius increases $\langle \tau \rangle$ is related to the variation of the friction parameter γ_0 with R . As R decreases, the acceptance probability of trial displacements of monomers inside the pore decreases because of an increasing likelihood that the move leads to overlap with the nanopore wall. This reduces the mobility for these monomers and therefore increases in γ_0 . This trend is illustrated in Fig. 4. From Eq. (17), it follows that the friction coefficient for the translocating polymer, γ , should also increase. The inset of Fig. 4 shows the variation of the friction coefficient for a polymer in an infinite cylindrical tube, γ_z , as a function of $N - 1$ for $R = 0.55$, where each γ_z value was determined by measuring $\langle \Delta z^2 \rangle$ as a function of time and us-

ing Eq. (12). Fitting the data using Eq. (13) yields the value of γ_0 . These results confirm the scaling relation of Eq. (13). [Note that the coupling between γ_0 and R is a consequence of the MC dynamics algorithm used. An alternative choice of trial moves for monomers in the pore, e.g. smaller displacements in the x - y direction compared to those along z , would allow decoupling of friction and pore radius.]

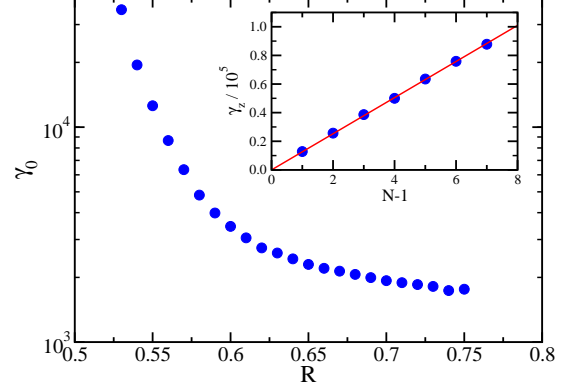


FIG. 4. Friction parameter, γ_0 , vs nanopore radius, R , for a polymer in an infinitely long cylindrical tube. The inset shows the friction coefficient γ_z , vs polymer length, $N - 1$, for a polymer in an infinite cylindrical tube of radius $R = 0.55$. The red curve is a fit to the linear function of Eq. (17)

A second factor contributing to slower translocation as R decreases can be understood from the effect of decreasing pore radius on the free energy profiles. As discussed in Ref. 46, the free energy is characterized by an oscillation with an amplitude, ΔF_{osc} , that increases with decreasing R . This is illustrated in Fig. 5(a), which shows profiles for a $N = 20$ polymer in a pore of length $L = 6$ for pore radii of $R = 0.55$ and $R = 0.8$. The origin of the oscillations is related to the nature of the variation with Q of the orientational entropy of the bonds at the two edges of the nanopore for this model. When the oscillation amplitude is of order $k_B T$ or larger, the translocation rate will be appreciably reduced. Thus, decreasing R increases ΔF_{osc} , which in turn increases $\langle \tau \rangle$. In addition to increasing the translocation times, the free energy oscillations can have other effects on the translocation dynamics. Figure 5(b) shows the history of Q for a single translocation event for a $N = 20$ polymer in a pore of length $L = 6$ and radius $R = 0.55$. The polymer clearly undergoes a diffusive type of motion while it is in the plateau region of the free energy profile in Fig. 5. Note, however, that the polymer tends to dwell longer at Q values close to the local free energy minima and jump rapidly over the free energy barriers. As R decreases, the oscillation amplitude increases, and the increase in the roughness of the landscape decreases the translocation rate.

In addition to its dependence on pore radius, the amplitude of the free energy oscillations also displays an interesting dependence on nanopore length. As is evi-

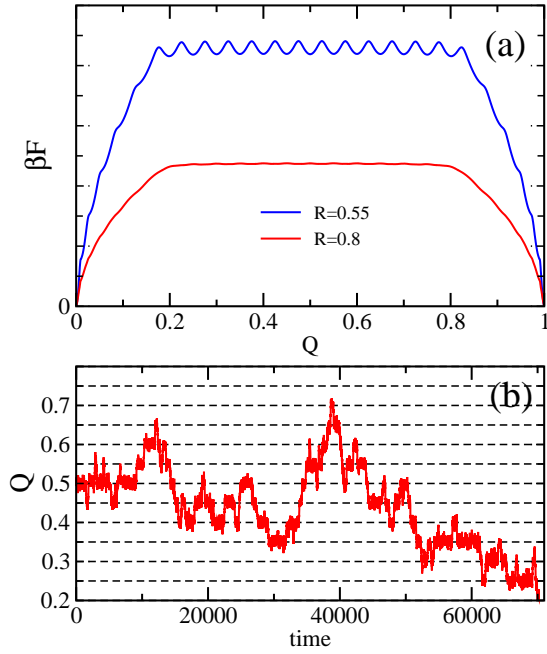


FIG. 5. (a) Translocation free energy profiles for a polymer of length $N = 20$ in a nanopore of length $L = 6$ for two different pore radii. (b) Q , vs time for an escape event for $R = 0.55$. The horizontal dashed lines mark the values of Q corresponding to local free energy minima.

dent in the inset of Fig. 6, the amplitude itself oscillates with L and has a period of $\Delta L = 1$, i.e. one bond length. The origin of this effect was explained in Ref. 46. For the case of $R = 0.55$ illustrated in the figure, the oscillation amplitude varies from negligible magnitude to a maximum of $\beta\Delta F_{\text{osc}} \approx 2.1$. The effect on the variation of $\langle\tau_1\rangle$ and $\langle\tau\rangle$ with L is shown in the figure and follows the expected pattern: for high values of ΔF_{osc} , translocation proceeds more slowly and the translocation times are high, while for nanopore lengths corresponding to low ΔF_{osc} , the translocation times are also low. This behaviour is expected to be independent of N , as long as the pore friction is sufficiently high. Results for $N = 100$ with $L = 2.917$ and $L = 2.333$ are consistent with this pattern (data not shown).

As explained in Section III, application of the FP formalism requires the value of the translocation diffusion coefficient or, equivalently, the friction coefficient, γ , to predict translocation times. Since the friction coefficient cannot easily be determined, we employ the procedure described earlier. The value of γ is chosen such that the mean translocation time, $\langle\tau_1\rangle$, calculated using Eq. (7) is equal to the value obtained directly from the dynamics simulations. This value can then be used in Eq. (17) to calculate N_{eff} , whose value should be close to the estimate in Eq. (15). Deviations from this estimate can be interpreted as a breakdown in the quasi-static condition and/or the assumption that pore friction is the dominant contribution to the total friction. The scaling

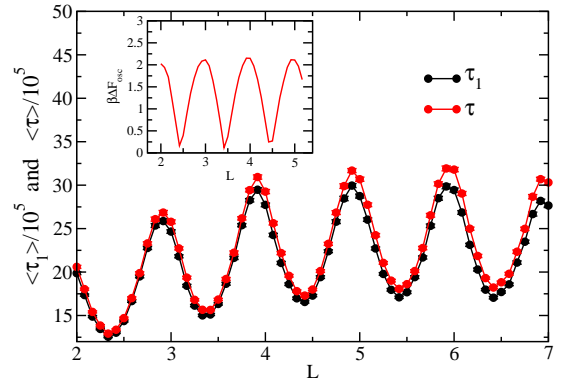


FIG. 6. Mean translocation times, $\langle\tau_1\rangle$ and $\langle\tau\rangle$, vs nanopore length, L , for a polymer of length $N = 20$ and a nanopore of radius $R = 0.55$. The inset shows the variation of the free energy oscillation amplitude, $\beta\Delta F_{\text{osc}}$ vs L .

$\gamma \propto N^2$ predicted by Eq. (17) provides another such test of quasi-equilibrium. Finally, this value of γ obtained by fixing $\langle\tau_1\rangle$ can be used in Eqs. (5) and (6) to predict the complete distribution of times, $g(\tau; Q_0)$.

Figure 7 shows the variation of the calculated N_{eff} with R for a $N = 20$ polymer in a pore of length $L = 3$. At the high end of the range of values of R shown, N_{eff} is significantly larger than the value of $N_{\text{eff}} \approx 5$ predicted by Eq. (15). The average number of monomers inside the pore was observed to increase only slightly with R , and so it does not account for this result. Consequently, it must be due to decrease in γ_0 with R , illustrated in Fig. 4. Generally, N_{eff} decreases with decreasing R for $R > 0.56$. Below this value, it is approximately constant, with a value $N_{\text{eff}} \approx 5.1$. This suggests that the quasi-static condition holds in this low- R regime. This interpretation is consistent with the variation of the scaling exponent α with R in Fig. 3, where the quasi-static limit value of $\alpha = 2$ is observed for $R = 0.55$. The inset shows the variation of N_{eff} with L for the same $N = 20$ polymer and a pore of radius $R = 0.55$. While N_{eff} does tend to increase with L , there is a superimposed oscillation with a period of $\Delta L = 1$. To help understand these results, the variation of N_{eff} with L was fit to the function

$$N_{\text{eff}} = L/\sigma + a_0 - a_1 \sin(2\pi L/\sigma). \quad (21)$$

This function provides a reasonable fit over the range of L considered, which yielded values of $a_0 = 2.18$ and $a_1 = 0.564$. Ignoring the oscillation, the prediction of $N_{\text{eff}} = L/\sigma + 2.18$ is roughly consistent with the prediction of Eq. (15). The origin of the oscillation is not completely understood at present but it may be a result of the MC algorithm employed. Note that the values of a_0 and a_1 are such that $N_{\text{eff}} \geq L/\sigma + 1.62$. The lower limit exceeds the average number of monomers inside the nanopore. Thus, the oscillation in N_{eff} is associated with the reduced mobility of monomers that lie outside the pore, the most significant of which lie in the zones of partial confinement near the pore edges ($-\sigma/2 < z < 0$

and $L < z < L + \sigma/2$). This effect is similar to that of the periodic variation of ΔF_{osc} with L illustrated in Fig. 6, which is also associated with the monomers near the edges.⁴⁶

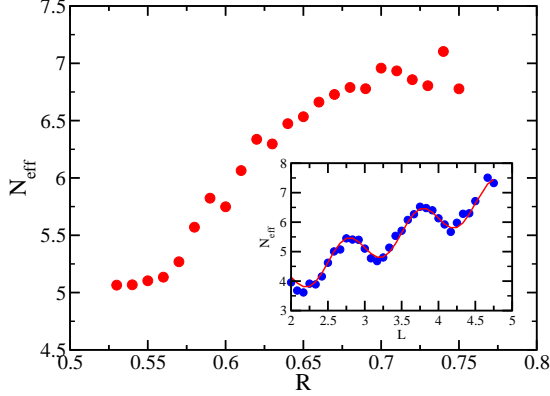


FIG. 7. Effective number of monomers in the nanopore, N_{eff} , vs pore radius for a polymer of length $N = 20$ in a nanopore of length $L = 3$. The inset shows the variation of N_{eff} with L for the same $N = 20$ polymer in a pore of radius $R = 0.55$. The red curve is a fit to Eq. (21).

Figure 8 shows translocation distributions calculated for a $N = 20$ polymer and a nanopore of dimensions $L = 3$ and $R = 0.55$. Distributions for $Q_0 = 0.3$ and $Q_0 = 0.5$ are shown. The figure also shows theoretical predictions for the distributions, calculated using the method described in Sections III and IV C. The friction coefficient γ was determined using Eq. (17) with $N_{\text{eff}} = 5.1$, the value obtained by constraining the predicted $\langle \tau_1 \rangle$ to be equal to that measured directly from the MC dynamics simulations for $Q_0 = 0.5$. The theoretical distributions are in excellent quantitative agreement with those obtained by simulation.

The translocation time distributions in Fig. 8 each display exponential tails at longer times. The origin of this feature can be understood in the context of simple diffusion between absorbing boundaries. For unforced translocation, the polymer spends most of its time moving over a relatively flat plateau of the free energy function, which is shown in the inset of the figure. When it reaches the plateau edge, the polymer quickly exits the pore during the pore-emptying stage, i.e., $\tau = \tau_1 + \tau_2 \approx \tau_1$, as described above. Neglecting the oscillations and the very slight overall negative curvature of the plateau, this process can be viewed approximately as simple diffusion with absorbing boundary conditions at $Q_a = 0.1$ and $Q_b = 0.9$. In this case, Eqs. (5) and (6) can be solved analytically, yielding:¹

$$g(\tau, Q_0) = \frac{2D_{\text{eff}}}{L_Q} \sum_{p=1}^{\infty} \beta_p [1 - \cos(\beta_p L_Q)] \sin(\beta_p (Q_0 - Q_a)) \exp\left[-\frac{D_{\text{eff}} \beta_p^2 L_Q^2}{\tau}\right]$$

where $\beta_p \equiv \pi p / L_Q$, and $L_Q \equiv Q_a - Q_b = 0.8$. For long first-passage time τ , the $p = 1$ term becomes dominant;

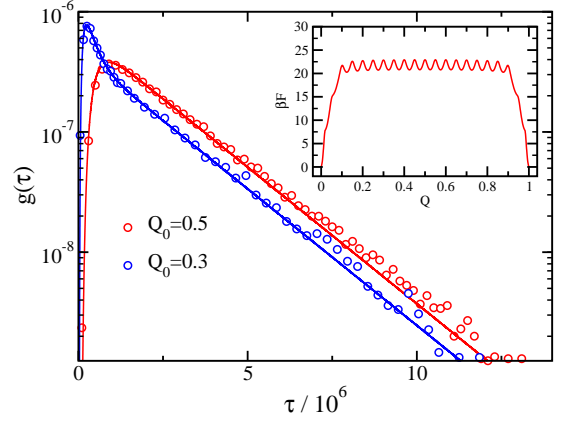


FIG. 8. Translocation time distributions for a polymer of length $N = 20$ and a nanopore of radius $R = 0.55$ and length $L = 3$. Distributions for two different Q_0 values are shown. The solid curves are theoretical predictions using $N_{\text{eff}} = 5.1$, which is obtained by setting the mean predicted time to be equal to the mean time from the dynamics simulations. The inset shows the free energy function for this system.

consequently,

$$g(\tau; Q_0) = C(Q_0) \exp(-\tau/\tau_c), \quad (23)$$

where

$$C(Q_0) \equiv \frac{4\pi D_{\text{eff}}}{L_Q^2} \sin(\pi((Q_0 - Q_a)/L_Q)), \quad (24)$$

and where the time constant, τ_c , is given by

$$\tau_c = L_Q^2 / (\pi^2 D_{\text{eff}}). \quad (25)$$

Thus, the exponential decay time is predicted to be independent of Q_0 , which is consistent with the data in the figure. Fitting the data in the exponential region to the function

$$g(\tau) = C' \exp(-\tau/\tau'_c) \quad (26)$$

yields $\tau'_c \approx 1.98 \times 10^6$. Using this value in Eq. (25), we estimate $D_{\text{eff}} \approx 3.2 \times 10^{-8}$. Of course, this approximation is strictly valid for a perfectly flat free energy curve. The corrugated structure of the free energy plateau slows down the rate of diffusion, and thus this value is expected to be lower than the value of D calculated using the methods described in Section III. Using Eqs. (16) and (17) with a value $N_{\text{eff}} = 5.1$ yields a value of $D = 4.84 \times 10^{-8}$, which is greater than D_{eff} , as expected. The fit also yields $C' = 6.7 \times 10^{-7}$ for $Q_0 = 0.5$, and $C' = 4.5 \times 10^{-7}$ for $Q_0 = 0.3$. These values are approximately consistent with the values predicted using Eq. (25) of $C(Q_0 = 0.5) = 6.3 \times 10^{-7}$ and $C(Q_0 = 0.3) = 4.4 \times 10^{-7}$. The small discrepancies arise from the approximations employed.

For the distributions shown in Fig. 8, it is evident that the mean translocation time for $Q_0 = 0.3$ is lower than the mean time for $Q_0 = 0.5$. This is an illustration of a

general result: the closer the polymer is initially situated to either one of the pore exits, the shorter the translocation time. This arises because the polymer exits more frequently at the closer pore boundary, and the shorter distance reduces the first passage time. The longer time required to reach the more distant exit is offset by the diminished probability of reaching that exit. This is consistent with the predictions for simple diffusion between absorbing boundaries.¹ It also effects a shift of the entire distribution to shorter times.

Figure 9 shows the variation with Q_0 of the probability of a *trans* side exit. As the initial position is moved closer to the *cis* side, i.e. as Q_0 decreases, the probability of a *trans* exit decreases, and the *cis* exit probability increases accordingly. The theoretical curve was calculated using Eq. (10), with $Q_a = 0.1$ and $Q_b = 0.9$, the bounds of the free energy plateau shown in the inset of Fig. 8. The theoretical prediction is in excellent agreement with the simulation probabilities. The observed variation of π_{trans} with initial position corresponds closely to the prediction for a diffusive process with a constant free energy between two absorbing boundaries, where the variation is exactly linear.¹ The slight deviation from linearity observed in Fig. 9 arises from the overall slight negative curvature of the (rough) free energy landscape evident in the inset in Fig. 8.

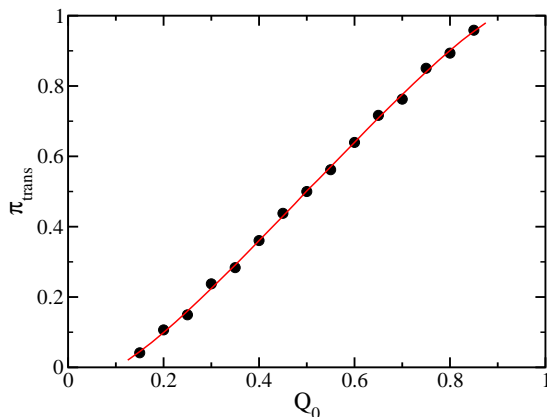


FIG. 9. Translocation probability, π_{trans} vs initial coordinate Q_0 for a polymer of length $N = 20$ and a nanopore of radius $R = 0.55$ and length $L = 3$. The symbols are data calculated directly from the MC dynamics simulations, and the solid line is a theoretical prediction using Eq. (10).

Figure 10 shows translocation time distributions calculated for three different polymer lengths using a nanopore with $L = 3$ and $R = 0.55$ and an initial coordinate of $Q_0 = 0.5$. As the polymer length increases, the distribution tends to broaden and the mean value increases. The theoretical distributions overlaid on the simulation data were all calculated using a friction coefficient, γ , obtained using Eq. (17) with $N_{\text{eff}} = 5.1$. As explained in Section III, the value of N_{eff} is expected to depend on the nanopore dimensions, but not on the polymer length. The excellent agreement between the theoretical distribu-

tions and those calculated by MC dynamics simulations using the same N_{eff} is consistent with this expectation.

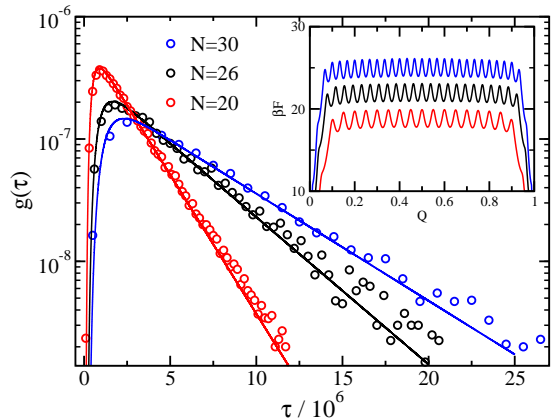


FIG. 10. Translocation time distributions for polymers of lengths $N = 20, 26$ and 30 , and a nanopore of radius $R = 0.55$ and length $L = 3$. The solid curves are theoretical predictions using $N_{\text{eff}} = 5.1$. The inset shows the free energy functions for the three systems. The functions have been vertically shifted to prevent overlap for visual clarity.

Figure 11 shows a comparison of translocation distribution times for nanopore lengths of $L = 3$ and $L = 2.5$, for the case where the polymer length is $N = 20$ and the nanopore radius is $R = 0.55$. The distribution is shifted to lower times for the shorter nanopore. The theoretical curves shown in the figure show excellent agreement with the simulation data. Note that the theoretical curve for $L = 2.5$ was calculated using $N_{\text{eff}} = 4.6$, a value that is consistent with the estimate in Eq. (15). A fit of the exponential tail of the $L = 2.5$ distribution yielded a time constant of $\tau'_c = 1.135 \times 10^6$. As seen in the figure inset, the free energy function is much smoother over the plateau region for $L = 2.5$ than for $L = 3$. In addition, the width of the plateau is approximately the same, i.e. $L_Q \approx 0.8$ in each case. Employing the model of free diffusion between absorbing boundaries at $Q = 0.1$ and 0.9 for the case of $L = 2.5$, Eq. (25) yields a value of $D_{\text{eff}} = 5.7 \times 10^{-8}$, which is very close to the value $D = 5.48 \times 10^{-8}$ predicted using Eqs. (16) and (17). This is exactly the consistency expected for a smooth, flat free energy function, and stands in contrast to the discrepancy between similarly calculated values of D_{eff} and D for $L = 3$ discussed above in the context of Fig. 8. It follows that much of the reduction in the translocation time upon decreasing the nanopore length from $L = 3$ to $L = 2.5$ is accounted for by decreasing roughness of the free energy function; a smaller contribution arises from the small decrease in N_{eff} and corresponding small increase in D .

Figure 12 shows translocation time distributions for a polymer that translocates out of a spherical cavity, the system illustrated in Fig. 1(b). The cavity radius is $R_c = 3$, and as before, $N = 20$, $L = 3$, and $R = 0.55$. Distributions for three different Q_0 are shown. Compar-

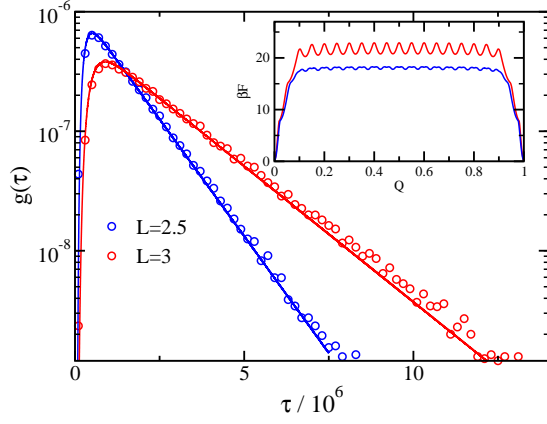


FIG. 11. Translocation time distributions for a nanopore of radius $R = 0.55$ and length $L = 3$. The polymer started midway through the pore with $Q_0 = 0.5$. Distributions for two different nanopore lengths are shown. The solid curves are theoretical predictions using $N_{\text{eff}} = 5.1$ for $L = 3.0$ and $N_{\text{eff}} = 4.6$ for $L = 2.5$.

ing the results with those of Fig. 8 for the flat barrier system shows that translocation times are slightly lower in the spherical cavity system. The origin of this effect is clear from a comparison of the free energy functions, shown in the figure inset. The confinement of the polymer in the cavity breaks the symmetry and leads to a free energy gradient. The resulting entropic driving force pushes the polymer to the *trans* side and reduces the time taken for the polymer to exit the nanopore.

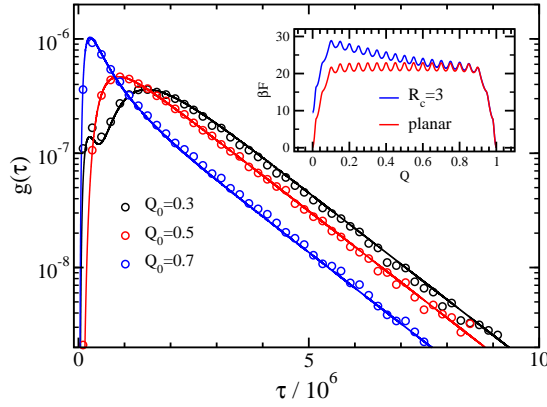


FIG. 12. Translocation time distributions for the spherical cavity system as illustrated in Fig. 1(b) for a cavity radius of $R_c = 3$. In addition, $R = 0.55$, $L = 3$ and $N = 20$. The theoretical curves were calculated as described in the text, using $N_{\text{eff}} = 5.6$. The inset shows the free energy function used in these theoretical calculations as well that used in calculations for the planar geometry.

The asymmetry in the free energy function means that $Q_0 = 0.3$ and $Q_0 = 0.7$ no longer have the same distributions, unlike the case for the symmetric flat-barrier system of Fig. 1(a). Instead, there is a monotonic decrease in the distribution mean times as the starting point of the

polymer is placed closer to the *trans* side of the nanopore (i.e. larger Q_0). The bias introduced by the entropic driving force causes the majority of translocation events associated with a polymer exit on the *trans* side of the pore. The closer to the *trans* side the polymer starts, the faster will be its exit. Note that this trend must inevitably reverse for sufficiently low Q_0 , i.e. if the polymer is almost complete inside the *cis* cavity, in which case the polymer may exit very rapidly into the spherical cavity.

The theoretical distributions shown in Fig. 12 are in excellent agreement with the simulation data. Note that the theoretical distribution for the spherical cavity system shown in the figure was calculated using $N_{\text{eff}} = 5.6$, somewhat larger than the value of $N_{\text{eff}} = 5.1$ employed for the flat-barrier system. As discussed above, N_{eff} is expected to depend only on L , which has the same value ($L = 3$) as that used in the flat barrier simulations. The slightly higher value of N_{eff} could be a result of out-of-equilibrium effects which arise from more rapid translocation due to the entropic driving force, as well as an increase in the relaxation time of the section of the polymer inside the spherical cavity. If so, then D and γ would likely exhibit a dependence on polymer length. As a check, we calculated the translocation time distributions for a longer polymer, $N = 30$, for an otherwise identical system. The theoretical predictions are in comparably good quantitative agreement with the distributions calculated from the dynamics simulations for the same value of N_{eff} (data not shown). This suggests that the difference in the values of N_{eff} for the two systems is not an out-of-equilibrium effect. More likely, the effect arises from the curvature of the cavity wall in the vicinity of the *cis* entrance to the nanopore. The curvature should lead to a slightly more crowded region near the entrance, which will lead to a slightly lower acceptance rate in the MC algorithm due to an increased likelihood of particle overlap. This in turn leads to a decrease in the monomer mobility near the entrance and consequently a slightly larger γ and N_{eff} . It has already been noted in the discussion above regarding the data in Fig. 7 how sensitive the pore friction can be to very small changes in the nanopore characteristics.

The FP predictions of translocation time distributions are in excellent quantitative agreement with those measured using MC dynamics method for the hard-potential model described in Section II. In order to demonstrate the generality of this result, we present preliminary results for a repulsive Lennard-Jones chain model. The details of the model are essentially the same as in Ref. 77, except that nanopore of finite length is used. The free energy function used in the FP calculation was calculated as in Ref. 46, and Brownian dynamics simulations were used to measure the distributions. Quasi-static conditions were achieved by increasing the friction coefficient of monomers inside the pore, γ_p , relative to that for monomers outside, γ_0 . Figure 13 shows results for $\gamma_p/\gamma_0 = 16$, for which there is excellent quantitative agreement between theory and simulation. The inset

shows that the measured N_{eff} approaches the expected value for sufficiently large γ_p/γ_0 . The results demonstrate that the FP methodology provides a valid description of quasi-static translocation dynamics for this commonly used simulation model. Further details will be presented in a future study.

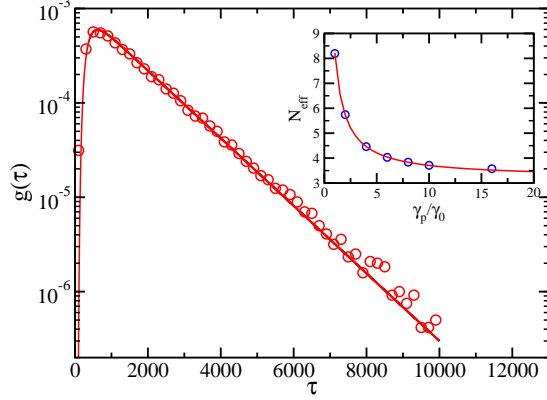


FIG. 13. Translocation time distribution for a repulsive LJ chain for the nanopore geometry of Fig. 1(a) calculated using Brownian dynamics simulations. Here, $\gamma_p/\gamma_0 = 16$, $R = 0.65$, $L = 3$, and $N = 20$. The solid line is the theoretical curve calculated using the FP formalism. The inset shows the variation of N_{eff} with γ_p/γ_0 .

VI. DISCUSSION

In this work, we have studied the translocation dynamics of a simple polymer/nanopore model system using Monte Carlo dynamics simulations and the Fokker-Planck formalism. The emphasis was on the quasi-static regime, in which the FP formalism provides a valid approach for describing translocation. While many theoretical studies have employed this approach, almost all have used approximate analytical forms for the free energy function. In our study, we use free energy functions calculated directly using a MC multiple histogram method for the same model used in the dynamics simulations. The translocation time distributions calculated using these functions thus provide a much better test of this theoretical approach than would otherwise be possible.

For the MC dynamics algorithm employed here, the key parameter governing the dynamical regime is the nanopore radius, R . As noted in a previous study,⁷⁷ decreasing R can slow the translocation rate in a manner that leads to a decrease in the translocation time scaling exponent, α . In the present case, this happens in part by effectively increasing the friction of the polymer in the pore. For sufficiently low R , the translocation rate decreased to the point that a value of $\alpha = 2$ was observed, indicating that the quasi-static regime was attained. This effect is similar to that observed in Ref. 51, in which

decreasing the solvent viscosity was used to attain the same exponent value. In each case, quasi-equilibrium is observed when the ratio of the translocation time to the conformational relaxation times of the *cis* and *trans* chain sections is sufficiently high. Muthukumar has noted that this is the relevant dynamical regime for experiments of DNA translocation through α -hemolysin pores.¹

Knowledge of the translocation free energy functions can provide valuable insight into the quantitative trends of the translocation dynamics. A useful illustration in this study is the effect of oscillations in the functions that occur for sufficiently small pore radius, R .⁴⁶ The translocation time is generally longer for systems with a higher free energy oscillation amplitude. Interestingly, the oscillation amplitude itself can be very sensitive to the nanopore length, L , as is evident in Fig. 6, which in turn leads to a sensitive dependence of the translocation time on L . While it is unlikely that oscillations arising from the same physical origin are present in the systems studied experimentally⁸⁸ this effect may be highly relevant to interpretation of results from other simulation studies, many of which use qualitatively similar models to that employed here. Since the oscillations are associated with the orientational freedom of only two polymer segments localized at the nanopore edges, the effect of slowing the translocation rate may even be present in cases where the *trans* and/or *cis* chain sections are out of equilibrium. Consequently, small changes in the nanopore geometry (such as L , here) could lead to significant changes in the translocation times, with corresponding changes in the scaling exponent, even outside the quasi-static regime. Such effects may account in part for the wide range of scaling exponents reported in various simulation studies. This underscores the importance of calculating accurate free energy functions to aid in the interpretation of dynamics simulation data.

Translocation time distributions for systems determined to be in the quasi-static regime were calculated using the FP formalism with measured free energy functions. The calculations assume that the nanopore friction is the dominant contribution to the overall friction coefficient for the translocation process. The distributions were calculated using a coefficient γ which was characterized by the parameter N_{eff} , the effective number of monomers whose motion is strongly affected by nanopore confinement. In the case of unforced translocation, we investigated the effects of varying polymer length, N , nanopore length, L , and the initial position of the polymer, Q_0 . In addition, we measured distributions for polymers translocating out of a spherically confined space, a feature that gives rise to an entropic force that drives translocation. The calculated distributions were generally in excellent quantitative agreement with those obtained directly from dynamics simulations for physically meaningful values of N_{eff} . Preliminary results of calculations using a repulsive LJ chain model and Brownian dynamics simulations yielded comparably good agreement.

In this study, calculations were carried out mainly for short polymer chains. This was due to the considerable computational effort required to obtain very accurate free energy functions and translocation time distributions from the simulations. In future work, we will investigate the effectiveness of FP formalism in describing translocation dynamics of much longer polymers. Another important issue not adequately addressed in this study is the effect of a driving force, which plays an essential role in DNA translocation experiments and whose effects have been extensively investigated in other simulation studies. Though we have briefly considered the effect of an entropic driving force in this work, a driving force associated with an potential energy gradient across the nanopore is not suitable for the MC dynamics algorithm employed here.⁸⁷ In a future study, we will examine this effect using Langevin and Brownian dynamics simulations. In addition, we will more thoroughly elucidate the regime within which the quasi-static approximation is sufficiently valid to justify using the FP formalism. This regime is expected to show a complex dependence on the polymer length, the conformational relaxation times of the chain, pore friction, the driving force strength, as well subtle features of the free energy functions. This work will also be extended to using more realistic molecular models to provide a more meaningful comparison with experimental systems. The long term goal of this research is to provide accurate predictions of translocation times using precisely calculated free energy functions within a well defined regime of validity.

ACKNOWLEDGMENTS

J.M.P. would like to thank Sheldon B. Opps for helpful discussions. This work was supported by the National Research Council of Canada (NSERC). We are grateful to the Atlantic Computational Excellence Network (ACEnet) for use of their computational facilities.

¹M. Muthukumar, *Polymer Translocation* (CRC Press, Boca Raton, 2011).

²B. Alberts, A. Johnson, J. Lewis, M. Raff, K. Roberts, and P. Walters, *Molecular Biology of the Cell*, 5th ed. (Garland Science, New York, 2008).

³H. Lodish, A. Berk, C. A. Kaiser, M. Krieger, A. Bretscher, H. Ploegh, A. Amon, and M. P. Scott, *Molecular Cell Biology*, seventh ed. (W. H. Freeman and Company, New York, 2012).

⁴J. J. Kasianowicz, E. Brandin, D. Branton, and D. W. Deamer, *Proc. Natl. Acad. Sci. U.S.A.* **93**, 13770 (1996).

⁵S. Bezrukov, I. Vodyanoy, R. Brutyan, and J. Kasianowicz, *Macromolecules* **29**, 8517 (1996).

⁶M. Akeson, D. Branton, J. Kasianowicz, E. Brandin, and D. Deamer, *Biophys. J.* **77**, 3227 (1999).

⁷A. Meller, L. Nivon, E. Brandin, J. Golovchenko, and D. Branton, *Proceedings of the National Academy of Sciences* **97**, 1079 (2000).

⁸A. Meller, *J. Phys.: Condens. Matter* **15**, R581 (2003).

⁹H. Wang, J. Dunning, A. Huang, J. Nyamwanda, and D. Branton, *Proceedings of the National Academy of Sciences of the United States of America* **101**, 13472 (2004).

- ¹⁰T. Z. Butler, J. H. Gundlach, and M. A. Troll, *Biophys. J.* **90**, 190 (2006).
- ¹¹C. T. A. Wong and M. Muthukumar, *J. Chem. Phys.* **128**, 154903 (2008).
- ¹²C. T. A. Wong and M. Muthukumar, *J. Chem. Phys.* **133**, 045101 (2010).
- ¹³J. Li, M. Gershow, D. Stein, E. Brandin, and J. Golovchenko, *Nature Mater.* **2**, 611 (2003).
- ¹⁴P. Chen, J. Gu, E. Brandin, Y. R. Kim, Q. Wang, and D. Branton, *Nano Lett.* **4**, 2293 (2004).
- ¹⁵D. Fologea, J. Uplinger, B. Thomas, D. McNabb, and J. Li, *Nano Lett.* **5**, 1734 (2005).
- ¹⁶D. Fologea, M. Gershow, B. Ledden, D. McNabb, J. Golovchenko, and J. Li, *Nano Lett.* **5**, 1905 (2005).
- ¹⁷A. J. Storm, C. Storm, J. Chen, H. Zandbergen, J.-F. Joanny, and C. Dekker, *Nano Lett.* **5**, 1193 (2005).
- ¹⁸A. Storm, J. Chen, H. Zandbergen, and C. Dekker, *Physical Review E* **71**, 051903 (2005).
- ¹⁹R. Purnell, K. Mehta, and J. Schmidt, *Nano Letters* **8**, 3029 (2008).
- ²⁰D. Branton *et al.*, *Nat. Biotechnol.* **26**, 1146 (2008).
- ²¹B. M. Venkatesan and R. Bashir, *Nat. Nanotech.* **6**, 615 (2011).
- ²²M. Wanunu, *Phys. Life Rev.* **9**, 125 (2012).
- ²³S. Kowalczyk, D. Wells, A. Aksimentiev, and C. Dekker, *Nano Lett.* **12**, 1038 (2012).
- ²⁴A. Milchev, *J. Phys.: Condens. Matter* **23**, 103101 (2011).
- ²⁵W. Sung and P. J. Park, *Phys. Rev. Lett.* **77**, 783 (1996).
- ²⁶M. Muthukumar, *J. Chem. Phys.* **111**, 10371 (1999).
- ²⁷M. Muthukumar, *Phys. Rev. Lett.* **86**, 3188 (2001).
- ²⁸M. Muthukumar, *J. Chem. Phys.* **118**, 5174 (2003).
- ²⁹E. Slonkina and A. B. Kolomeisky, *J. Chem. Phys.* **118**, 7112 (2003).
- ³⁰C. Y. Kong and M. Muthukumar, *J. Chem. Phys.* **120**, 3460 (2004).
- ³¹D. Keijan, Z. Furu, C. Dongqin, and Y. Zengliang, *Biochem. Biophys. Res. Commun.* **341**, 139 (2006).
- ³²A. Mohan, A. B. Kolomeisky, and M. Pasquali, *J. Chem. Phys.* **133**, 024902 (2010).
- ³³S. Yang and A. V. Neimark, *J. Chem. Phys.* **136**, 214901 (2012).
- ³⁴C. Rasmussen, A. Vishnyakov, and A. Neimark, *J. Chem. Phys.* **137**, 144903 (2012).
- ³⁵S. Mirigian, Y. Wang, and M. Muthukumar, *J. Chem. Phys.* **137**, 064904 (2012).
- ³⁶H. Qian, L.-Z. Sun, and M.-B. Luo, *J. Chem. Phys.* **137**, 034903 (2012).
- ³⁷M. G. Gauthier and G. W. Slater, *J. Chem. Phys.* **128**, 065103 (2008).
- ³⁸M. G. Gauthier and G. W. Slater, *J. Chem. Phys.* **128**, 205103 (2008).
- ³⁹H. W. de Haan and G. W. Slater, *J. Chem. Phys.* **134**, 154905 (2011).
- ⁴⁰P.-G. de Gennes, *Scaling Concept in Polymer Physics* (Cornell University Press, London, 1979).
- ⁴¹L.-Z. Sun, W.-P. Cao, and M.-B. Luo, *J. Chem. Phys.* **131**, 194904 (2009).
- ⁴²Y.-C. Chen, C. Wang, Y.-L. Zhou, and M.-B. Luo, *J. Chem. Phys.* **130**, 054902 (2009).
- ⁴³C. Rasmussen, A. Vishnyakov, and A. Neimark, *J. Chem. Phys.* **135**, 214109 (2011).
- ⁴⁴D. Frenkel and B. Smit, *Understanding Molecular Simulation: From Algorithms to Applications*, 2nd ed. (Academic Press, London, 2002) Chap. 7.
- ⁴⁵M. Fatehi Hassanabad and J. M. Polson, *Phys. Can.* **65**, 126 (2009).
- ⁴⁶J. M. Polson, M. Fatehi Hassanabad, and A. C. M. McCaffrey, *J. Chem. Phys.* **138**, 024906 (2013).
- ⁴⁷J. Chuang, Y. Kantor, and M. Kardar, *Phys. Rev. E* **65**, 011802 (2001).
- ⁴⁸Y. Kantor and M. Kardar, *Phys. Rev. E* **69**, 021806 (2004).
- ⁴⁹D. Panja, G. T. Barkema, and R. C. Ball, *J. Phys.: Condens.*

- Matter **19**, 432202 (2007).
- ⁵⁰J. L. A. Dubbeldam, A. Milchev, V. G. Rostiashvili, and T. A. Vilgis, Phys. Rev. E **76**, 010801(R) (2007).
- ⁵¹H. W. de Haan and G. W. Slater, J. Chem. Phys. **136**, 154903 (2012).
- ⁵²J. L. A. Dubbeldam, A. Milchev, V. G. Rostiashvili, and T. A. Vilgis, EPL **79**, 18002 (2007).
- ⁵³H. Vocks, D. Panja, G. T. Barkema, and R. C. Ball, J. Phys.: Condens. Matter **20**, 095224 (2008).
- ⁵⁴T. Sakaue, Phys. Rev. E **76**, 021803 (2007).
- ⁵⁵T. Sakaue, Phys. Rev. E **81**, 041808 (2010).
- ⁵⁶T. Saito and T. Sakaue, Eur. Phys. J. E **34**, 135 (2011).
- ⁵⁷P. Rowghanian and A. Y. Grosberg, J. Phys. Chem. B **115**, 14127 (2011).
- ⁵⁸J. L. A. Dubbeldam, V. G. Rostiashvili, A. Milchev, and T. A. Vilgis, Phys. Rev. E **85**, 041801 (2012).
- ⁵⁹T. Ikonen, A. Bhattacharya, T. Ala-Nissila, and W. Sung, Phys. Rev. E **85**, 051803 (2012).
- ⁶⁰T. Ikonen, A. Bhattacharya, T. Ala-Nissila, and W. Sung, J. Chem. Phys. **137**, 085101 (2012).
- ⁶¹T. Ikonen, A. Bhattacharya, T. Ala-Nissila, and W. Sung, arXiv preprint arXiv:1211.7043 (2012).
- ⁶²A. Milchev, K. Binder, and A. Bhattacharya, J. Chem. Phys. **121**, 684 (2004).
- ⁶³S. Tsuchiya and A. Matsuyama, Phys. Rev. E **76**, 011801 (2007).
- ⁶⁴K. Luo, T. Ala-Nissila, and S.-C. Ying, J. Chem. Phys. **124**, 034714 (2006).
- ⁶⁵J. K. Wolterink, G. T. Barkema, and D. Panja, Phys. Rev. Lett. **96**, 208301 (2006).
- ⁶⁶S. Guillouzie and G. W. Slater, Phys. Lett. A **359**, 261 (2006).
- ⁶⁷I. Huopaniemi, K. Luo, T. Ala-Nissila, and S.-C. Ying, Phys. Rev. E **75**, 061912 (2007).
- ⁶⁸D. Panja, G. T. Barkema, and R. C. Ball, J. Phys.: Condens. Matter **20**, 075101 (2008).
- ⁶⁹D. Wei, W. Yang, X. Jin, and Q. Liao, J. Chem. Phys. **126**, 204901 (2007).
- ⁷⁰K. Luo, S. T. T. Ollila, I. Huopaniemi, T. Ala-Nissila, P. Pommorski, M. Karttunen, S.-C. Ying, and A. Bhattacharya, Phys. Rev. E **78**, 050901(R) (2008).
- ⁷¹V. V. Lehtola, R. P. Linna, and K. Kaski, Phys. Rev. E **78**, 061803 (2008).
- ⁷²V. V. Lehtola, R. P. Linna, and K. Kaski, EPL **85**, 58006 (2009).
- ⁷³K. Luo, T. Ala-Nissila, S.-C. Ying, and R. Metzler, EPL **88**, 68006 (2009).
- ⁷⁴M. G. Gauthier and G. W. Slater, Phys. Rev. E **79**, 021802 (2009).
- ⁷⁵A. Bhattacharya, W. H. Morrison, K. Luo, T. Ala-Nissila, S.-C. Ying, A. Milchev, and K. Binder, Eur. Phys. J. E **29**, 423 (2009).
- ⁷⁶F. Kapahnke, U. Schmidt, D. W. Heermann, and M. Weiss, J. Chem. Phys. **132**, 164904 (2010).
- ⁷⁷H. W. de Haan and G. W. Slater, Phys. Rev. E **81**, 051802 (2010).
- ⁷⁸J. L. A. Dubbeldam, V. G. Rostiashvili, A. Milchev, and T. A. Vilgis, Phys. Rev. E **83**, 011802 (2011).
- ⁷⁹K. Luo, I. Huopaniemi, T. Ala-Nissila, and S.-C. Ying, J. Chem. Phys. **124**, 114704 (2006).
- ⁸⁰K. Luo and R. Metzler, Phys. Rev. E **82**, 021922 (2010).
- ⁸¹A. Bhattacharya and K. Binder, Phys. Rev. E **81**, 041804 (2010).
- ⁸²J. Feng, Y. Shang, L. Zhou, H. Liu, and Y. Hu, Chin. J. Chem. Eng. **20**, 231 (2012).
- ⁸³A. Cacciuto and E. Luitjen, Phys. Rev. Lett. **96**, 238104 (2006).
- ⁸⁴K. Zhang and K. Luo, J. Chem. Phys. **136**, 185103 (2012).
- ⁸⁵V. V. Lehtola, K. Kaski, and R. P. Linna, Phys. Rev. E **82**, 031908 (2010).
- ⁸⁶D. Panja and G. T. Barkema, J. Chem. Phys. **132**, 014902 (2010).
- ⁸⁷Consider the drift-diffusion process for a polymer in an infinite tube with a constant energy gradient. The polymer driving force is $\propto N$. On the other hand, from Eq. (13), the friction coefficient associated with diffusion is $\gamma_z = D_z/k_B T \propto N - 1$. This leads to an inconsistency between the friction coefficient measured from diffusion and that measured from the polymer drift velocity. This is also true for tubes of finite length. In the Langevin dynamics algorithm, $\gamma_z = D_z/k_B T \propto N$, and this problem does not arise.
- ⁸⁸As noted in Ref. 46, the oscillations in the free energy require very sharp boundaries at the nanopore edge. Nanopores used in experiments are unlikely to satisfy this requirement. However, oscillations arising from energetic interactions between the polymer and the nanopore wall could very well be present.